THE JOURNAL OF BIOLOGICAL CHEMISTRY VOL. 289, NO. 28, pp. 19704–19713, July 11, 2014


# Two Amino Acid Residues Confer Different Binding Affinities of Abelson Family Kinase Src Homology 2 Domains for Phosphorylated Cortactin*

Received for publication, February 6, 2014, and in revised form, May 15, 2014 Published, JBC Papers in Press, June 2, 2014, DOI 10.1074/jbc.M114.556480

**Stacey M. Gifford**[‡1,2], **Weizhi Liu**[§1,3], **Christopher C. Mader**[¶], **Tiffany L. Halo**[‖], **Kazuya Machida**[**4], **Titus J. Boggon**[§‡‡5], **and Anthony J. Koleske**[‡‡§§¶¶6]

*From the Departments of [‡]Molecular Biophysics and Biochemistry, [§]Pharmacology, [¶]Cell Biology, and [‖]Chemistry, the [‡‡]Yale Cancer Center, [§§]Interdepartmental Neuroscience Program, and [¶¶]Department of Neurobiology, Yale University, New Haven, Connecticut 06520 and the [**]Department of Genetics and Developmental Biology, Raymond and Beverly Sackler Laboratory of Genetics and Molecular Medicine, University of Connecticut Health Center, Farmington, Conneticut 06030*

**Background:** Abl family kinases bind different targets despite highly similar sequences.
**Results:** Two residues in the Src homology (SH) 2 domain regulate binding to phosphorylated cortactin and modulate cell protrusion.
**Conclusion:** The Arg SH2 domain binds with higher affinity than the Abl SH2 domain to phosphorylated cortactin.
**Significance:** Slight sequence changes can cause affinity differences, leading to important functional changes in cellular interactions.

**The closely related Abl family kinases, Arg and Abl, play important non-redundant roles in the regulation of cell morphogenesis and motility. Despite similar N-terminal sequences, Arg and Abl interact with different substrates and binding partners with varying affinities. This selectivity may be due to slight differences in amino acid sequence leading to differential interactions with target proteins. We report that the Arg Src homology (SH) 2 domain binds two specific phosphotyrosines on cortactin, a known Abl/Arg substrate, with over 10-fold higher affinity than the Abl SH2 domain. We show that this significant affinity difference is due to the substitution of arginine 161 and serine 187 in Abl to leucine 207 and threonine 233 in Arg, respectively. We constructed Abl SH2 domains with R161L and S187T mutations alone and in combination and find that these substitutions are sufficient to convert the low affinity Abl SH2 domain to a higher affinity "Arg-like" SH2 domain in binding to a phospho-cortactin peptide. We crystallized the Arg SH2 domain for structural comparison to existing crystal structures of the Abl SH2 domain. We show that these two residues are important determinants of Arg and Abl SH2 domain binding specificity. Finally, we expressed Arg containing an "Abl-like" low affinity mutant Arg SH2 domain (L207R/T233S) and find that this mutant, although properly localized to the cell periphery, does not support wild type levels of cell edge protrusion. Together, these observations indicate that these two amino acid positions confer different binding affinities and cellular functions on the distinct Abl family kinases.**

Abelson (Abl)[7] family non-receptor tyrosine kinases are important regulators of actin dynamics and coordinate changes in cell morphology and migration (1). The N-terminal halves of Abl and the Abl-related gene (Arg), containing their Src homology 3 (SH3), Src homology 2 (SH2), and kinase domains, are nearly 90% identical, whereas their C-terminal extensions, which contain cytoskeletal-binding domains and scaffolding functions, are much less conserved (1, 2). Despite sequence similarities and known roles in actin cytoskeletal regulation, Abl and Arg regulate differential zones of actomyosin contractility in fibroblasts (3). Moreover, Abl and Arg have differential roles in neuronal dendrite maintenance and in the support of invadopodial function in invasive breast cancer cells (4, 5).

In addition to their differences in expression, subcellular localization, and function, Arg and Abl interact with different substrates *in vivo* (3, 6–9). For example, we have previously shown that whereas both Abl and Arg phosphorylate the actin polymerization regulator cortactin *in vitro*, Arg alone interacts with cortactin via a set of scaffolding interactions that are essential for both proteins to promote cell edge protrusion during cell adhesion (10, 11). Furthermore, Arg, but not Abl, is critical for cortactin phosphorylation during actin-based protrusion in breast cancer cells (5). This selectivity can be explained in part by the high-affinity binding of the cortactin SH3 domain to an extended Pro-*X*-*X*-Pro-*X*-*X*-Pro motif that

* This work was supported, in whole or in part, by National Institutes of Health Grants GM100411 and AI075133 (to T. J. B.), NS39475, GM100411, and CA133346 (to A. J. K.), and pilot grants from the Connecticut Breast Health Initiative and Women's Health Research at Yale (to T. J. B. and A. J. K.).
[1] Both authors contributed equally to this work.
[2] Supported by American Heart Association Founders Affiliate Predoctoral Fellowship 11PRE7450039.
[3] Present address: College of Marine Life Sciences, Ocean University of China, 5 Yushan Rd., Qingdao 266003, People's Republic of China.
[4] Supported by National Institutes of Health Grant R01 CA82258.
[5] To whom correspondence may be addressed: Dept. of Pharmacology, 333 Cedar St., New Haven, CT 06520. Tel.: 203-785-2943; Fax: 203-785-5494; E-mail: titus.boggon@yale.edu.
[6] To whom correspondence may be addressed: Dept. of Molecular Biophysics and Biochemistry, Yale University, New Haven, CT 06520. Tel.: 203-785-5624; Fax: 203-785-7979; E-mail: anthony.koleske@yale.edu.

[7] The abbreviations used are: Abl, Abelson; Arg, Abl-related gene; SH2, Src homology 2; SH3, Src homology 3; Fmoc, *N*-(9-fluorenyl)methoxycarbonyl; pY, phosphotyrosine.

occurs in Arg but not Abl (10). A recent crystal structure suggests that the cortactin SH3 domain engages the first three of these prolines along an extended type II polyproline helix (12).

During cell adhesion, cortactin SH3 domain binding to Arg is essential for subsequent phosphorylation of cortactin by Arg at one or more of three previously identified tyrosine phosphory10, 13, 14). This phosphorylation creates a binding site for the Arg SH2 domain, a discrete second interaction interface between the two proteins, although the exact phosphotyrosines required for binding were previously unknown (15). This finding raised the question of whether the Arg SH2 domain might also confer additional specificity to the Arg-cortactin interactions. SH2 domains bind phosphotyrosines with a high degree of selectivity, which is dictated by surrounding residues. In particular, three residues C-terminal to the phosphotyrosine determine SH2 domain binding specificity (16, 17). Within the SH2 domain itself, there are three binding pockets that confer specificity for each of these binding target residues as well as several loops, which govern binding pocket accessibility (18, 19).

We report here that of the three previously described cortactin tyrosine phosphorylation sites ($Tyr^{421}$, $Tyr^{466}$, $Tyr^{482}$), only peptides corresponding to the phosphorylated $Tyr^{421}$ and $Tyr^{466}$ sites bind with significant affinities to the Arg SH2 domain. We also find that despite nearly 90% domain sequence identity, the Arg SH2 domain binds the phosphorylated cortactin $Tyr^{421}$ peptide with over 10-fold greater affinity than the Abl SH2 domain. We show that this binding specificity is due to two residues that differ between Abl and Arg, arginine 161 and serine 187 in Abl, which correspond to leucine 207 and threonine 233 in Arg, respectively (Fig. 2*A*). We provide the first crystal structure of the Arg SH2 domain and show that $Leu^{207}$ is located near the P + 1 binding pocket and $Thr^{233}$ is on the EF loop previously shown to mediate access to the P + 3 binding pocket (18). Finally, we show that although these residues do not affect Arg localization to the cell periphery, they are critical for mediating actin-based cell edge protrusion in fibroblasts.

## EXPERIMENTAL PROCEDURES

*Molecular Cloning of Recombinant SH2 Domains*—Human Arg ($Val^{131}$–$Tyr^{238}$) and Abl ($Asn^{121}$–$Val^{226}$) SH2 domains were subcloned into pGEX6p-1 (GE Healthcare) using BamHI and EcoRI restriction sites. Abl SH2 G144L, R161L/S187T, and S188A single and double mutants were generated by PCR and also cloned into pGEX6p-1. Arg L207R/T233S-EYFP was generated using site-directed mutagenesis of wild type Arg N1-EYFP (Clontech Laboratories, Inc.). EYFP, wild type Arg EYFP, and Arg L207R/T233S-EYFP were subcloned into the retroviral expression vector PK1 (10).

*Protein Purification for Crystallization*—Initial protein expression and purification were carried out in *Escherichia coli* BL21(DE3) cells and induced at 20 °C overnight with 0.1 mM isopropyl β-D-1-thiogalactopyranoside. After induction, the cells were pelleted, resuspended, and lysed using a freeze-thaw protocol and sonication with the presence of 1 mg/ml of lysozyme. Following sonication and centrifugation (20,000 × *g*) at 4 °C for 30 min, the resulting supernatant was incubated with glutathione-Sepharose 4B beads (GE Healthcare) for 4 h at 4 °C. 20 bead volumes of PBS buffer were then used to wash the resin before being incubated with PreScission protease (GE Healthcare) at 4 °C overnight to remove the GST tag. The Arg SH2 protein was further purified on a Superdex 75 column in 20 mM Hepes (pH 7.5) buffer containing 100 mM NaCl, 1 mM EDTA, 1 mM DTT. The protein was concentrated to 20 mg/ml for crystallization.

*Peptide Synthesis and 5-Carboxyfluorescein Labeling*—Peptides corresponding to phosphorylated tyrosine sites 421 (SSPIpYEDAA), 466 (SEPVpYETTE), or 482 (EDDTpYDGYE) of mouse cortactin were synthesized on a 30-μmol scale with a Liberty 12-channel microwave synthesizer (CEM Corp., Matthews, NC) using standard Fmoc chemistry. Following removal of the final Fmoc protecting group, the resin was washed with dimethylformamide and methylene chloride alternatively for a total of 16 washes and dried for 20 min under nitrogen gas. The peptides were N terminally labeled overnight with a mixture comprised of 5-carboxyfluorescein, succinimidyl ester (8 mg, 0.017 mmol), and diisopropylethylamine (24 μl, 17.8 mg, 0.138 mmol) in 1.5 ml of dimethylformamide.

Labeled peptide was treated with a cleavage mixture of 2.5% (v/v) 3,6-dioxa-1,8-octanedithiol, 2.5% (v/v) $H_2O$, 2.5% (v/v) triisopropylsilyl in TFA (50% power at 400 W maximum, 38 °C ramp for 2 min, hold for 30 min; followed by treatment with fresh mixture at 50% power, 400 W maximum, 38 °C, ramp 2 min, hold 5 min). Crude peptide was lyophilized and reconstituted in acetonitrile/water (1:1). Synthesis efficiency was assessed by MALDI-TOF analysis of the crude reaction mixture followed by purification to homogeneity by reverse phase HPLC. A second round of MALDI-TOF reconfirmed peak sample homogeneity. Following purification, peptide was lyophilized and stored in the dark at −20 °C.

*Fluorescence Polarization Measurements*—SH2 domains were dialyzed into binding buffer (50 mM Hepes, pH 7.25, 150 mM NaCl, 0.01% Nonidet P-40, 5% glycerol) and a 30-μl volume serially diluted into pre-chilled 384-well low flange black flat bottom non-binding microplates (Corning) while on ice. 5 μl of 35 nM fluorescent peptide dissolved in binding buffer was added to each well (final concentration 5 nM), mixed 5 times by pipetting, and plates were incubated at 4 °C for 40 min. Fluorescence polarization experiments were performed with an Analyst AD (Molecular Devices, Sunnyvale, CA) spectrofluorimeter. Each well was excited using 485 nm light and emission was read at 530 nm. Fluorescence polarization was measured 1 mm from the bottom of each well with an integration time of 560 ms. All experiments were conducted in triplicate. The change in fluorescence polarization was normalized such that maximum change for each condition ($B_{max}$) was set at an arbitrary value of 100 for ease of comparison (Figs. 1 and 2). Normalized values were graphed and fit to a single binding site hyperbola using GraphPad Prism.

*Crystallization and Structure Determination*—Arg SH2 domain crystals were grown in conditions containing 15–17% PEG 4000, 0.2 M sodium acetate, and 100 mM Tris-HCl, pH 8.5. Crystals were grown within 3 days at room temperature by hanging drop vapor diffusion. Before data collection, the crystals were flash frozen in liquid nitrogen using the crystallization conditions supplemented with 20% PEG 400. Crystallographic data were collected at beamline X6A of the National Synchro-

tron Light Source (Table 1), and data were processed using HKL2000 (20).

The structure of the Arg SH2 domain was determined by molecular replacement using the program PHASER (21). The SH2 domain from Abl (Protein Data Bank code 3K2M (22)) was used as a search model and yielded a translation *Z*-score of 17.2. Automated model building using ARP/wARP (23) built 95 residues, thus avoiding potential problems with model bias. Manual model building and refinement were then conducted using COOT (24) and Refmac5 (25) from the CCP4 suite, respectively. Restrained refinement with anisotropic *B*-factors and automatic water placement with ARP_waters (26) were used in later rounds of refinement. A total of 100 water molecules were added during refinement. The final structure was validated using PROCHECK (27) and MolProbity (28) and the secondary structure was assigned using the computer program, DSSP (29). All residues fall within the favored or allowed regions of the Ramachandran plot. Arg SH2 maintains a typical SH2-fold with 2 major $\alpha$-helices ($\alpha$A and $\alpha$B) and 7 $\beta$-strands ($\beta$A to $\beta$G). The structure is deposited in the Protein Data Bank under accession code 4EIH.

*Cell Culture and Retroviral Expression*—Wild type and $arg^{-/-}$ fibroblasts were maintained as previously described (30). EYFP, Arg-EYFP, and Arg L207R/T233S-EYFP were expressed via retroviral expression and 1.0 $\mu$g/ml of puromycin selection as previously described (10). Expression levels of wild type and retrovirally expressed Arg proteins were determined by immunoblotting 75 $\mu$g of cell lysate as determined with a BCA kit (Pierce) with a mouse anti-Arg antibody and control mouse monoclonal antibody against HSP70 (3A3) (Santa Cruz). Expression levels were quantified using Quantity One software (Bio-Rad).

*Immunoprecipitation and Western Blotting*—Fibroblasts were serum starved for 1 h then plated on 10 $\mu$g/ml of bovine fibronectin-coated plates (Sigma), blocked with 1% BSA, and allowed to adhere for 45 min. Cells were washed with PBS and lysed in 50 mM Hepes, pH 7.5, 1% Nonidet P-40, 150 mM KCl, 5% glycerol, 0.5 mM metavanadate, 0.5 mM orthovanadate, 2 mM NaF, and complete protease inhibitors. 0.75 mg/ml of soluble lysate was incubated with protein A/G beads and anti-cortactin 4F11 antibody for 24 h at 4 °C. Supernatant and precipitant samples were immunoblotted with anti-phosphotyrosine 4G10 antibody and anti-cortactin 4F11 antibody. Phosphorylation levels were quantified and normalized to total cortactin levels using Quantity One software (Bio-Rad).

*Immunofluorescence Microscopy*—Fibroblasts were plated on 10 $\mu$g/ml of bovine fibronectin-coated coverslips (Sigma), blocked with 1% BSA, and allowed to adhere for 30 min. Cells were fixed with 4% PFA for 20 min at room temperature and permeabilized with 0.5% Triton X-100 for 10 min. Cells were then stained with a mouse anti-GFP monoclonal antibody (Rockland), which cross-reacts with EYFP, followed with Alexa Fluor 647 goat anti-mouse antibody (Invitrogen), as well as Alexa Fluor 488 phalloidin (Invitrogen). Cells were imaged on a model TE2000-S Nikon microscope with a ×20 or 100 objective with NIS Elements (Nikon).

To control for possible bleed-through of the Arg/Arg mutant-YFP signal into the actin channel, $arg^{-/-}$ fibroblasts expressing EYFP were stained only with antibodies to EYFP and Alexa 647 goat anti-mouse secondary antibody or only with phalloidin-Alexa 488 alone and were imaged at both 501 and 654 nm. No bleed-through of the Arg/Arg mutant-YFP signal was observed in the 501 channel, and no actin staining was observed in the 654 nm channel. These experiments indicate that the EYFP signal from the expressed protein is disrupted during fixation and processing.

*Quantification of Cell Circularity*—Cells stained for phalloidin and imaged at ×100 were traced peripherally in ImageJ. Circularity was quantified using the analyze shape descriptors function in the ImageJ Software package, which can be described as a function of cell area and cell perimeter.

$$C = 4\pi\left[\frac{area}{(perimeter)^2}\right] \qquad \text{(Eq. 1)}$$

*Adhesion-dependent Cell Edge Protrusion Assays and Kymography*—Adhesion-dependent fibroblast cell edge protrusion assays were performed 30 min after cells were plated on 10 $\mu$g/ml of bovine fibronectin (Sigma)-coated MatTek dishes (MatTek Corp.) and imaged as described previously (10). Kymographic analysis of cell edge protrusion was performed as described previously using ImageJ software and GraphPad Prism (10, 30).

*Measurements of Cell Spreading*—Fibroblasts were plated on 10 $\mu$g/ml of bovine fibronectin (Sigma)-coated MatTek dishes (MatTek Corp.). Time-lapse images of spreading cells were recorded for 30 min. The cell area was measured at 0, 10, 20, and 30 min by peripherally tracing and quantifying each cell in ImageJ.

*Statistics*—Unless otherwise noted, grouped samples were subjected to two-way analysis of variance followed by post-hoc Student's *t* tests where described (* = $p < 0.05$; ** = $p < 0.01$; *** = $p < 0.001$; **** = $p < 0.0001$). All graphs display mean ± S.E.

## RESULTS

*Arg and Abl Bind Cortactin Phosphotyrosines 421 and 466, but Not 482*—We used fluorescence anisotropy to measure the binding affinity of wild type Abl and Arg SH2 domains for fluoresceinated cortactin peptides corresponding to the sequences surrounding phosphorylated $Tyr^{421}$, $Tyr^{466}$, and $Tyr^{482}$ (Fig. 1*D*). We found that the Arg SH2 domain binds with highest affinity to the $Tyr(P)^{421}$ peptide, binds with a 2-fold lower affinity to $Tyr(P)^{466}$ peptide, and does not bind detectably to $Tyr(P)^{482}$ peptide (Fig. 1, *A* and *C*). The Abl SH2 domain showed a similar trend in binding affinity for the three phosphorylated cortactin peptides (Fig. 1, *B* and *C*). Neither SH2 domain binds unphosphorylated cortactin peptides with any detectable affinity.

*Arg and Abl SH2 Domains Differ in Only a Few Non-conserved Amino Acids*—Despite nearly identical sequences, the Arg SH2 domain shows a greater than 10-fold higher affinity in comparison to the Abl SH2 domain for the cortactin $Tyr(P)^{421}$ peptide (Fig. 1). ClustalW was used to perform sequence align-

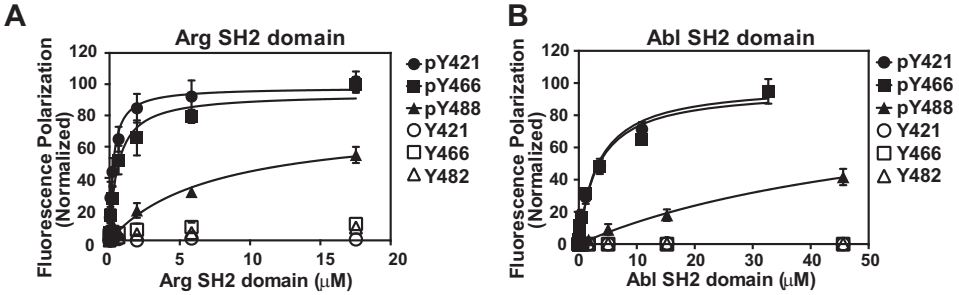


C

| SH2 Domain | $K_d$ (μM) pY421 | pY466 | pY488 | Y421 | Y466 | Y482 |
|---|---|---|---|---|---|---|
| Arg | 0.26±0.07 | 0.58±0.15 | >7.27 | N.B. | N.B | N.B |
| Abl | 3.33±0.53 | 3.27±0.74 | >61.92 | N.B. | N.B | N.B |

D

pY421 - SSPIpYEDAA
pY466 - SEPVpYETTE
pY482 - EDDTpYDGYE

FIGURE 1. **Arg and Abl SH2 domains bind phosphorylated cortactin peptides Tyr(P)$^{421}$ and Tyr(P)$^{466}$, but not Tyr(P)$^{482}$.** Quantification of binding between Arg (*A*) and Abl (*B*) SH2 domains and peptides corresponding to phosphorylated (*pY*) and non-phosphorylated (*Y*) cortactin tyrosines 421, 466, and 482. Experiments were performed in triplicate and points represent mean ± S.E. (*error bars* may be obscured by data points). Data were fit using a one-site specific binding curve (GraphPad Prism) normalized to saturation ($B_{max}$). *C,* table of binding affinities and mean ± S.E. from binding curves in *A* and *B*, peptides that showed no binding are labeled as *N.B*. *D,* sequences of cortactin peptides used in *A* and *B*.

ment of Arg and Abl SH2 domains. These two SH2 domain sequences are 90% identical, with two non-conserved residues, two semi-conserved residues, and six conserved residues (Fig. 2*A*). Of these 10 residues, three are located in regions within or near the binding pocket region of the SH2 domain (Fig. 3*A*). These residues are Leu$^{207}$, Thr$^{233}$, and Ala$^{234}$ in Arg, which correspond to Arg$^{161}$, Ser$^{187}$, and Ser$^{188}$ in Abl. Leu$^{190}$ in Arg and the corresponding residue in Abl, Gly$^{144}$, are also non-conserved but are located outside of the binding pocket and we therefore predicted this substitution would have little effect on the binding affinity.

*Two Amino Acid Residues in the Arg and Abl SH2 Domains Confer Different Binding Affinities for a Phosphorylated Cortactin Peptide*—We measured the binding affinity of Abl SH2 mutants with substitutions at the residues that differ from the Arg SH2 domain for the cortactin Tyr(P)$^{421}$ peptide. The Abl SH2 single mutants, G144L and S188A, showed no change in affinity from that of wild type Abl SH2 domain (Fig. 2, *C*, *D*, *G*, and *I*). However, both Abl SH2 R161L and S187T showed intermediate affinities for the Tyr(P)$^{421}$ peptide (Fig. 2, *E*, *F*, and *I*). In light of this partial increase in affinity, we hypothesized that the double mutation (R161L/S187T) of the Abl SH2 domain may confer the strong affinity observed in the wild type Arg SH2 domain. As hypothesized, the Abl double mutant (R161L/S187T) SH2 domain is able to bind the cortactin Tyr(P)$^{421}$ peptide with similar affinity to that observed for the wild type Arg SH2 domain (Fig. 2, *B*, *H*, and *I*). These data suggest that these two residues determine the relative binding affinities of Arg and Abl SH2 domains for the Tyr(P)$^{421}$ cortactin peptide.

*Structural Analysis of Arg SH2 Domain*—The structure of the Arg SH2 domain has never been solved crystallographically. In light of our affinity measurements (Fig. 2) we wondered whether there were structural explanations for both Arg SH2 domain specificity for Tyr(P)$^{421}$ and Tyr(P)$^{466}$ over Tyr(P)$^{482}$, and the higher affinity of Arg SH2 domain for cortactin when compared with Abl SH2 domain. We therefore conducted a structural analysis of the Arg SH2 domain. We first purified the Arg SH2 domain and crystallized this domain in space group $C222_1$. We then determined the structure of the Arg SH2 domain to 1.2-Å resolution (Fig. 3*A*, Table 1). This allowed us to directly compare the Arg SH2 domain to the Abl SH2 domain (22, 31–34) and other previously determined type IA SH2 domain structures (35–39).

First, we compared the structure of the Arg SH2 domain with previously determined Abl crystal structures as well as an NMR structure of Arg SH2 domain (PDB codes 1OPK, 1OPL, 1AB2, 2ABL, 2ECD, 2FO0, and 3K2M) (22, 31–34). The crystal structure of the Arg SH2 domain shows root mean square deviations for C$\alpha$ atoms with these structures ranging from 0.75 to 1.55 Å (Fig. 3*B*). Overall these structures, including the NMR structure of the Arg SH2 domain, are extremely similar, however, there is distinct conformational flexibility for the BC loop, which is observed in conformations that vary by as much as 9 Å.

We next compared the Arg SH2 domain to other type 1A SH2 domain structures that have been determined in complex with phosphotyrosine peptides. These structures (*e.g.* for Lck (35, 40) and Src (39)) show that the peptide specificity is determined at the P + 3 location by a Tyr(P)[−][−]Ψ motif, where Ψ is a hydrophobic residue. This binding site is maintained in the Arg SH2 domain by formation of the phosphotyrosine binding pocket by residues Arg$^{180}$, Arg$^{198}$, Gln$^{206}$, Ser$^{208}$, Tyr$^{218}$, His$^{219}$, Tyr$^{220}$, and Arg$^{221}$, and formation of the P + 3 hydrophobic binding pocket by residues Val$^{232}$, Thr$^{233}$, Gly$^{254}$, and Leu$^{255}$. We conducted structural modeling by superposition of the Arg SH2 domain with the structure of Lck bound to an 11-residue phosphopeptide (EPQpYEEIPIYL) derived from the hamster polyoma middle-T antigen (PDB 1LCJ) (35) (Fig. 3*C*). The structural superposition clearly shows that a large residue at the P + 3 location would be incompatible with binding. This correlates well with the undetectable binding for the cortactin Tyr(P)$^{482}$ peptide, which has a tyrosine residue in the P + 3 location as compared with the Tyr(P)$^{421}$ and Tyr(P)$^{466}$ peptides (Fig. 1), which have alanine and threonine residues, respectively.

We then analyzed the locations of the residues that diverge between the Arg and Abl SH2 domains. We found that Arg

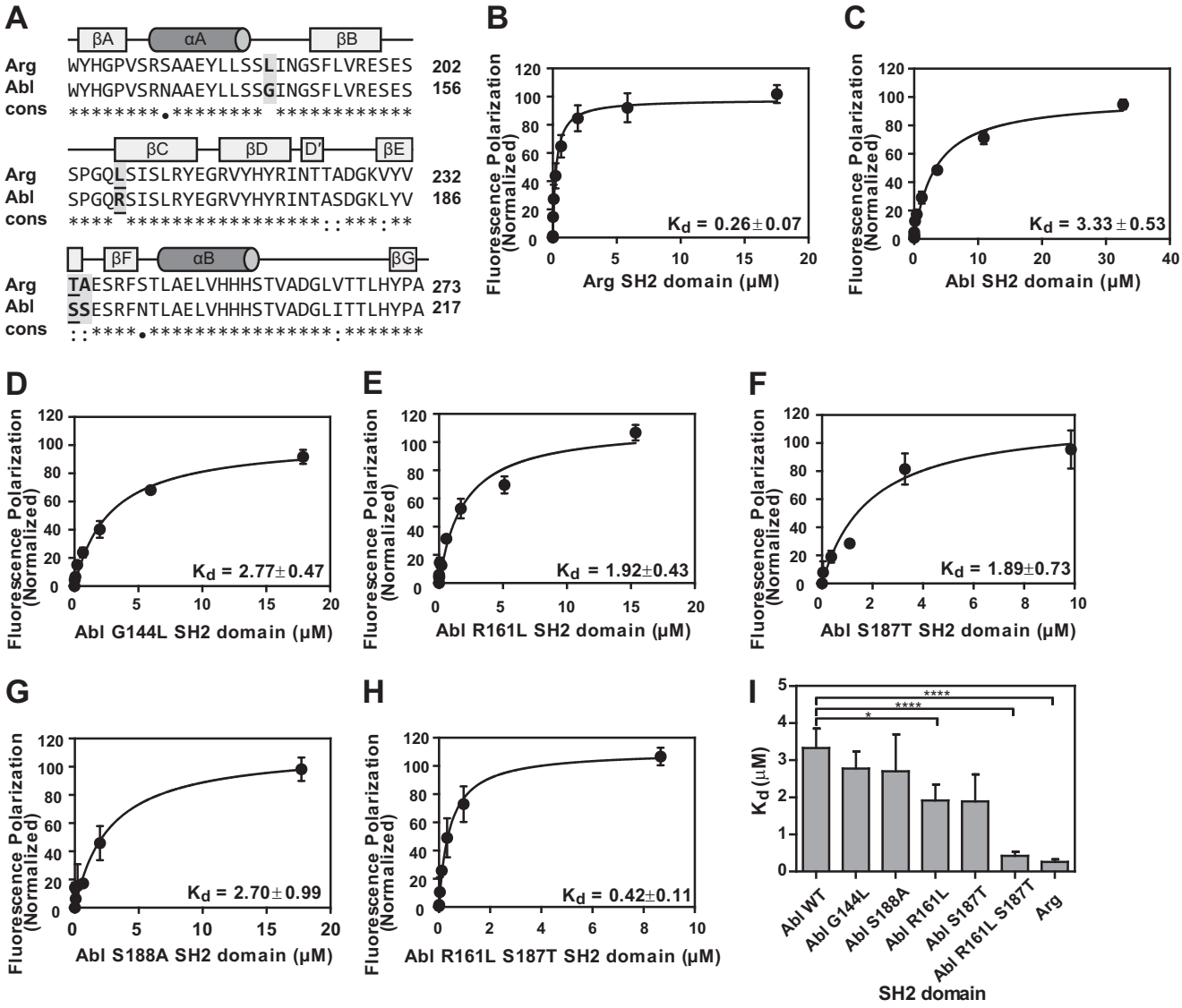


FIGURE 2. **Sequence alignment and binding analysis of SH2 domains for cortactin Tyr(P)$^{421}$ peptide.** *A,* sequence alignment of Arg SH2 and Abl SH2 domains using ClustalW. ClustalW conservation: *, identical; :, conserved; ●, semi-conserved. The secondary structure elements are assigned based on the Arg SH2 crystal structure with β-strands indicated as *boxes*, and α-helices as *cylinders*. Residues mutated in this study are highlighted with a *gray box* and the two residues important for binding affinity (Leu$^{207}$/Arg$^{161}$ and Thr$^{233}$/Ser$^{187}$) are *underlined*. *B–H*, quantification of binding between Arg SH2 domain (*B*), Abl SH2 domain (*C*), Abl G144L SH2 domain (*D*), Abl R161L SH2 domain (*E*), Abl S187T SH2 domain (*F*), Abl S188A SH2 domain (*G*), or Abl R161L/S187T SH2 domain (*H*) and cortactin Tyr(P)$^{421}$ phosphopeptide. Experiments were performed in triplicate and points represent mean ± S.E. (*error bars* may be obscured by data points). Data were fit using a one-site specific binding curve (GraphPad Prism) normalized to saturation ($B_{max}$). All binding affinities ($K_d$) are given in micromolar. *I,* statistical analysis of binding affinities determined from binding curves in GraphPad Prism. Values are mean ± S.E., *, $p < 0.1$; **, $p < 0.01$.

Leu$^{190}$/Abl Gly$^{144}$ residues are distal from the peptide binding cleft correlating well with our data showing that mutagenesis of these residues does not alter peptide binding specificity. Thr$^{233}$ is located in the Arg kinase EF loop and is proximal to the P + 3 peptide binding location, consistent with our data showing that the amino acid identity at this position affects peptide binding affinity. Notably, Leu$^{207}$ is part of the BC loop, but points away from the phosphotyrosine binding site. In structures of the Abl SH2 domain, the corresponding residue, Arg$^{161}$, can make a salt bridge to Glu$^{153}$, potentially impacting the conformation of the BC loop. However, in the Arg SH2 domain structure the presence of Leu$^{207}$ in this location results in a loss of the salt bridge and an orientation change in the side chain of the corresponding Glu$^{199}$ (Fig. 3*D*). We hypothesize that for the Abl double mutant (R161L/S187T), the loss of this salt bridge formation and potential alteration in BC loop conformation combined with an altered P + 3 pocket work in concert to allow increased binding affinity toward phosphorylated cortactin.

*Wild Type Arg-EYFP and Arg L207R/T233S-EYFP Both Localize to the Cell Periphery*—Wild type fibroblasts display dynamic cell edge protrusions as they adhere to fibronectin-coated surfaces (10, 30, 41). We have shown that the Arg SH2 domain binding to phosphorylated cortactin is critical for this process (10). To test if this high affinity interaction supported by residues Leu$^{207}$ and Thr$^{233}$ is relevant in cells we retrovirally expressed wild type Arg-EYFP or Arg L207R/T233S-EYFP in mouse *arg*$^{-/-}$ fibroblasts (Fig. 4, *A–C*). Cells fixed and stained for actin, and EYFP reveal that localization of Arg L207R/T233S-EYFP is similar to that of wild type Arg-EYFP in *arg*$^{-/-}$ fibroblasts and is enriched at the cell

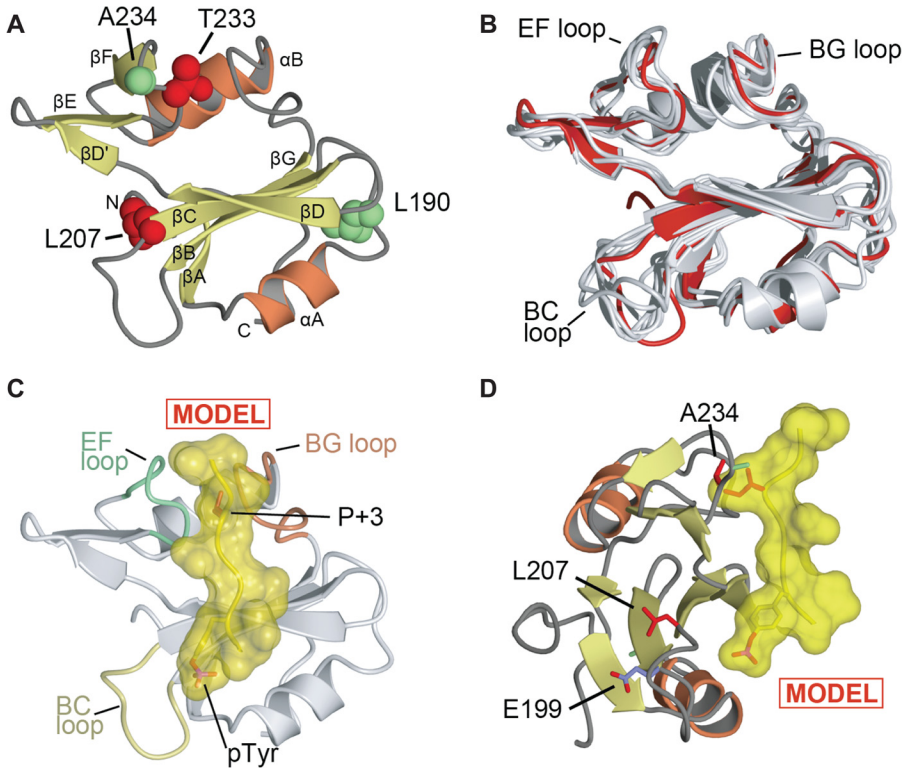


FIGURE 3. **Structural analysis of Arg SH2 domain.** *A*, overall view of the crystal structure of the Arg SH2 domain. α-Helices and β-strands are labeled. Arg residues Leu[190] and Ala[234] are shown as *spheres* and colored *green*. Arg residues Leu[207] and Thr[233] are shown as *spheres* and colored *red*. The structure is deposited in the Protein Data Bank under accession code 4EIH. *B*, superposition of determined structures of Arg and Abl SH2 domains. Arg SH2 domain (this study) is colored *red*, previously determined structures are shown in *gray* (PDB codes 1OPK, 1OPL, 1AB2, 2ABL, 2ECD, 2FO0, and 3K2M) (22, 31–34). The superposition was conducted using Topp (25). *C* and *D*, model of phosphotyrosine peptide binding to Arg SH2 domain. The model was generated by superposition of Arg SH2 with the Lck SH2-peptide (EPQpYEEIPIYL) complex (35). *C*, shows only the Arg SH2 domain and the location of the superposed peptide (in *yellow*). Structural diagrams generated using CCP4MG (48). *D*, shows an orientation rotated 90° with Arg residues Leu[207], Thr[233], and Glu[199] shown in stick format.

**TABLE 1**
**Crystallographic data collection and refinement statistics**

| | |
|---|---|
| **Data collection** | |
| Space group | $C222_1$ |
| Cell dimensions, *a*, *b*, *c* (Å) | 56.3, 81.9, 37.7 |
| Resolution (Å)[a] | 20.0-1.2 (1.24-1.20) |
| Unique reflections[a] | 25,814 |
| Completeness (%) | 93.9 (63.9) |
| $R_{sym}$ (%)[a] | 4.6 (23.7) |
| $Mn(I/\sigma)$[a] | 29.0 (5.3) |
| $R_{factor}$ (%) | 16.1 |
| Free $R_{factor}$ (%) | 18.1 |
| Residues built | 167–267 |
| Free *R* reflections (%) | 5 |
| Free *R* reflections No. | 1,302 |
| No. non-hydrogen protein atoms | 819 |
| No. water molecules | 100 |
| **Model quality** | |
| Root mean square deviation bond length (Å) | 0.014 |
| Root mean square deviation bond angles (°) | 1.54 |
| Mean *B*-factors | |
| Overall (Å$^2$) | 29.6 |
| Protein atoms (Å$^2$) | 23.8 |
| Water (Å$^2$) | 47.8 |
| Solvent (Å$^2$) | 22.7 |
| Ramachandran plot (%) favored/allowed/disallowed | 94.4/5.6/0 |

[a] Parentheses indicate the highest resolution shell.

periphery (Fig. 4*E*), suggesting that these residues do not impact localization within the cell. Control experiments (described under "Experimental Procedures") indicated that channel bleed-through of the Arg/Arg mutant and actin staining was not an issue (Fig. 4*F*).

Overall morphology, which we quantified as cell circularity, shows similarity in cell shape between wild type fibroblasts and $arg^{-/-}$ fibroblasts expressing wild type Arg-EYFP. Cells expressing mutant Arg L207R/T233S-EYFP appear similar in circularity to $arg^{-/-}$ fibroblasts and $arg^{-/-}$ fibroblasts expressing EYFP, suggesting that despite its proper localization, the mutant Arg does not support normal cell morphology (Fig. 4*D*).

*Arg Residues Leu[207] and Thr[233] Support Wild Type Level Cell Edge Protrusion Fibroblasts*—Wild type fibroblasts undergo dynamic cell edge protrusions as they adhere and spread on fibronectin-coated glass and Arg is critical for this behavior (10, 30, 41). To test if residues Leu[207] and Thr[233] are required to support adhesion-dependent cell edge protrusion, we recorded time-lapse images of wild type fibroblasts and $arg^{-/-}$ fibroblasts expressing EYFP, wild type Arg-EYFP, and Arg L207R/T233S-EYFP adhering to fibronectin-coated coverslips (Fig. 5). We quantified cell edge protrusive behavior using kymography as previously described (30) and find that wild type fibroblasts and $arg^{-/-}$ fibroblasts expressing wild type Arg-EYFP exhibit a high number of protrusions and retractions (Fig. 5, *A*, *C*, *E*, and *F*). In contrast, $arg^{-/-}$ fibroblasts expressing EYFP alone or expressing mutant Arg L207R/T233S-EYFP show a significant reduction in the number of protrusions and retractions (Fig. 5, *B*, *D*, *E*, and *F*), confirming that these residues are important for cell edge protrusion in fibroblasts. We do not see a significant difference in the

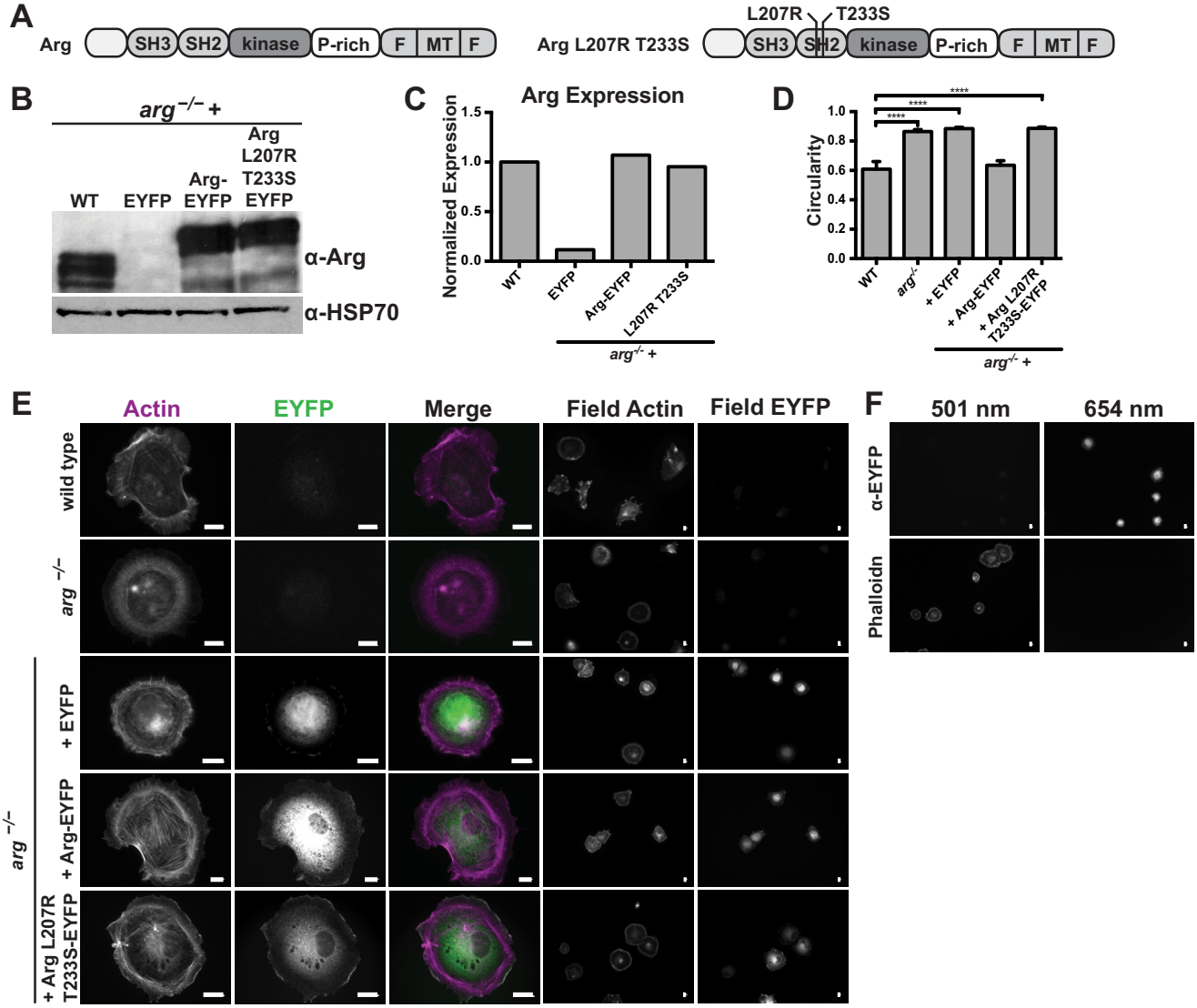


FIGURE 4. **Arg-EYFP and Arg L207R/T233S-EYFP localize to the cell periphery.** *A,* domain structure of full-length wild type Arg and mutant Arg L207R/T233S. *B,* immunoblot of cell lysates from wild type fibroblasts and $arg^{-/-}$ fibroblasts expressing EYFP, wild type Arg-EYFP, or Arg L207R/T233S-EYFP. Western blot with α-Arg antibody shows Arg expression levels compared with the control α-HSP70 blot. *C,* quantification of Arg expression from *B*. *D,* circularity of cells quantified from phalloidin-stained fibroblasts plated on fibronectin as shown in *E*. Values are mean ± S.E. for a minimum 15 cells per cell type, ****, $p < 0.0001$. *E,* immunostaining of wild type fibroblasts, $arg^{-/-}$ fibroblasts, and $arg^{-/-}$ fibroblasts expressing EYFP, wild type Arg-EYFP, or Arg L207R/T233S-EYFP for actin (*first column*) and EYFP (*second column*). Merged images (*third column*) show colocalization. The *fourth* and *fifth columns* show field images of multiple cells immunostained for actin and EYFP, respectively. *F,* control for channel bleed-through $arg^{-/-}$ fibroblasts expressing EYFP stained only with antibodies to EYFP and Alexa 647 secondary antibodies (*top row*) or with phalloidin-Alexa 488 alone (*bottom row*) and imaged at both 501 (*left column*) and 654 (*right column*) nm. *Scale bar* indicates 10 μm.

overall spreading area of cells, indicating that whereas dynamic cell edge protrusions are disrupted, overall area of the spread is not affected (Fig. 5*H*).

Efficient phosphorylation of cortactin by Arg relies on the Arg P*XX*P-cortactin SH3 domain interaction as well as an intact Arg kinase domain. These interactions should not be compromised in the Arg L207R/T233S-EYFP mutant. We immunoprecipitated cortactin from $arg^{-/-}$ fibroblasts, or $arg^{-/-}$ fibroblasts expressing EYFP, Arg-EYFP, or mutant Arg L207R/T233S-EYFP and immunoblotted for phosphotyrosine. Cortactin phosphorylation levels are reduced in $arg^{-/-}$ + EYFP fibroblasts, but $arg^{-/-}$ fibroblasts were reconstituted with Arg-YFP and Arg L207R/T233S-EYFP exhibited similar levels of cortactin phosphorylation (Fig. 5*G*).

We also hypothesized that a chimera of Arg containing the Abl R161L/S187T SH2 domain would rescue cell edge protrusion in a manner similar to wild type Arg. Unfortunately, these constructs did not express well in fibroblasts despite repeated attempts (data not shown).

## DISCUSSION

We show that Arg and Abl SH2 domains bind with high affinity to phosphorylated cortactin residues $Tyr^{421}$ and $Tyr^{466}$, but not $Tyr^{482}$. Despite nearly identical sequences, we find that the Arg and Abl SH2 domains bind phosphorylated cortactin with a nearly 10-fold difference in affinity. Interestingly, we find that two specific residues, $Arg^{161}$ and $Ser^{187}$ in Abl and $Leu^{207}$ and $Thr^{233}$ in Arg, mediate the difference in affinity of these

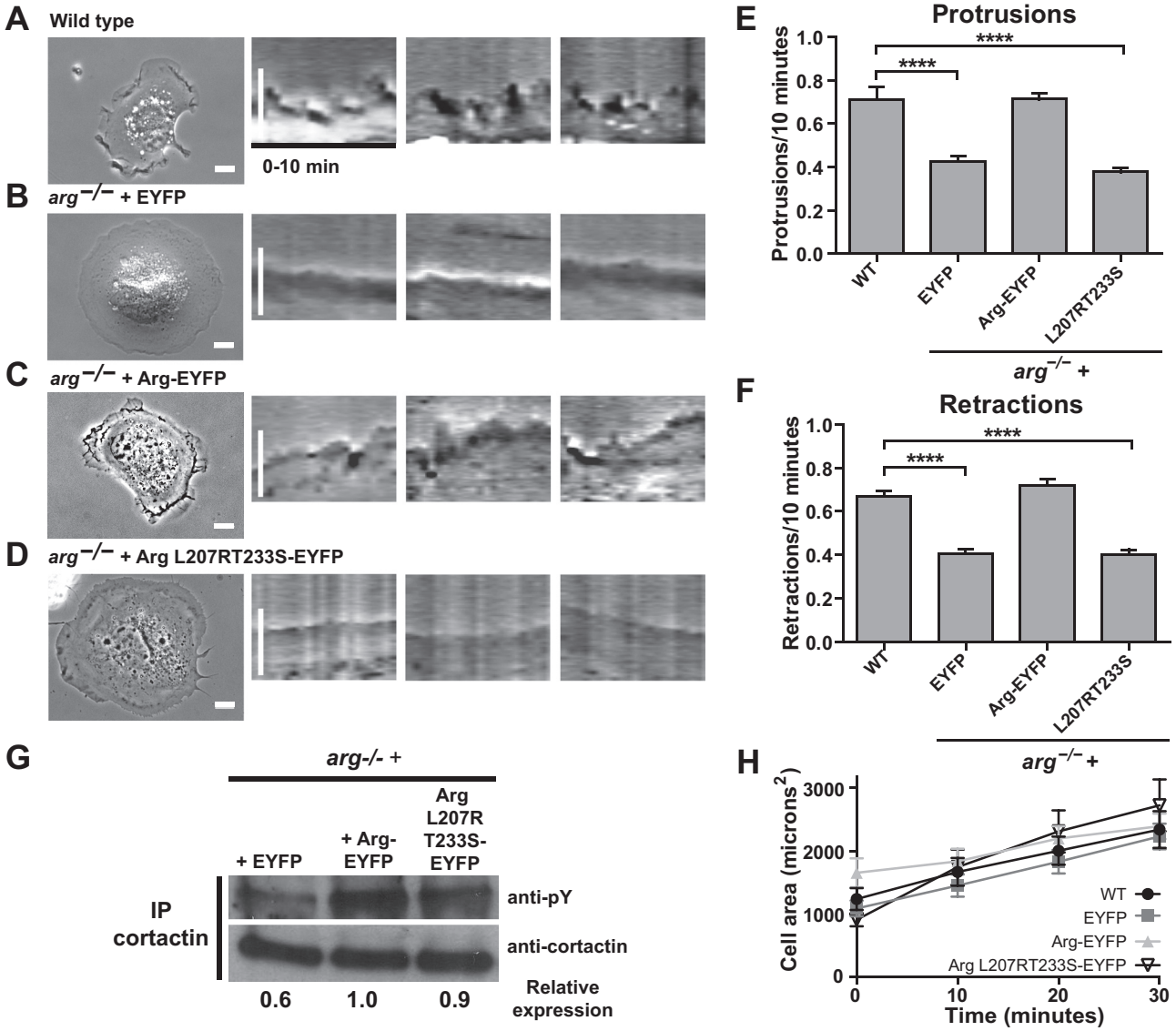


FIGURE 5. **Arg L207R/T233S-EYFP is unable to rescue cell edge protrusion in fibroblasts adhering to fibronectin.** *A–D*, phase images and 10-min kymographs of wild type fibroblasts (*A*) and $arg^{-/-}$ fibroblasts expressing EYFP (*B*), wild type Arg-EYFP (*C*), or Arg L207R/T233S-EYFP (*D*). *Scale bars* indicate 10 $\mu$m. Quantification of protrusions (*E*) and retractions (*F*) were measured over 10 min. Values are mean ± S.E., ****, $p < 0.0001$. *G*, phosphorylation levels of cortactin in $arg^{-/-}$ fibroblasts expressing EYFP, Arg-EYFP, or Arg L207R/T233S-EYFP. Cortactin was immunoprecipitated (*IP*) and Western blotted for phosphotyrosine. Cortactin phosphorylation is reduced in $arg^{-/-}$ + EYFP fibroblasts, but similar in $arg^{-/-}$ + Arg-EYFP and $arg^{-/-}$ + Arg L207R/T233S-EYFP cells. *H*, quantification of cell spreading. Cell area was measured at 0, 10, 20, and 30 min of spreading on fibronectin.

SH2 domains for phosphorylated cortactin. We provide a crystal structure of the Arg SH2 domain, which shows that these two residues are located near the binding pocket. Finally, we demonstrate that these two SH2 domain residues are functionally important to support cell edge protrusion.

Phosphorylation of cortactin residues $Tyr^{421}$ and $Tyr^{466}$ is required for actin polymerization in breast cancer cell invadopodia, whereas phosphorylation of the previously identified $Tyr^{482}$ is not (42). Furthermore, we previously showed that Arg phosphorylates cortactin on two of these tyrosines, $Tyr^{421}$ and $Tyr^{466}$ (10, 11). We support these observations by demonstrating that $Tyr(P)^{421}$ and $Tyr(P)^{466}$, but not $Tyr(P)^{482}$, interact with Arg and Abl SH2 domains. This is likely due to the inability of the Arg and Abl SH2 domain binding pocket to accommodate the bulky tyrosine residue found in the P + 3 site of the $Tyr(P)^{482}$ peptide. Similarly, only $Tyr^{421}$ and $Tyr^{466}$ are conserved in and important for regulation of the cortactin homolog HS1 (43).

We show that Arg and Abl SH2 domains bind phosphorylated cortactin with dramatically different affinities. Through biochemical and structural approaches, we identified Arg residues $Leu^{207}$ and $Thr^{233}$ as key mediators of this high affinity interaction. Although the difference in affinity does not impact Arg localization, it is important for proper cell edge protrusion. Arg localization to the cell periphery is conferred by its C-terminal cytoskeletal binding domains and its SH2 domain does not impact subcellular localization (44). Our data agree with these previous studies. These findings further reinforce the fact that despite sequence similarity, Arg and Abl have unique roles within the cell. Evolving interaction specificity through affinity is one mechanism by which kinases target specific substrates, and swapping SH2 domains between kinases has been shown to

alter the substrate profile from the wild type kinase (45). Our research suggests that this difference in affinity between Arg and Abl SH2 domains contributes to the different roles these two kinases play in the cell.

SH2 domains also play an important role in regulating processive phosphorylation of substrates with multiple phosphorylation sites (46) and SH2 domain binding preference has been shown to correlate well with phosphorylation site preference of the associated kinase (45, 47). It is possible that the Arg SH2 domain specificity for $Tyr(P)^{421}$ in cortactin potentiates efficient phosphorylation of a subsequent tyrosine residue, such as $Tyr^{466}$, leading to increased actin polymerization in invadopodia. This increased cortactin phosphorylation would lead to the up-regulation of actin polymerization in invadopodia. This mechanism may contribute to the fact that Arg, but not Abl, localizes to invadopodia in breast cancer cells and is essential for cortactin-mediated actin polymerization at these sites (5).

Previous studies show that selective interactions between Arg and cortactin underlie the ability of Arg to serve as a scaffold to support cortactin function during cell edge protrusion. Loss of the Arg SH2 domain-cortactin phosphotyrosine interaction leads to a reduction in cell edge protrusion (10). In relationship to these studies, we show that affinity of these interactions is an important determinant of whether or not they are able to perform their intended function in the cell. By expressing the mutant Arg L207R/T233S-EYFP in cells, we decrease the affinity between the Arg SH2 domain and phosphorylated cortactin and this decrease in affinity results in a failure of Arg to support wild type levels of cell edge protrusion. We also find that the circularity of cells expressing Arg L207R/T233S-EYFP is altered compared with wild type cells, reflecting a disruption of overall cytoskeletal structure and cell shape. Together, our results demonstrate the importance of two residues in the binding pocket of Arg and Abl SH2 domains for high affinity binding to phosphorylated cortactin and further highlight the non-redundant function of these two related kinases in cellular processes.

*Acknowledgments—Vivian Stojanoff and Jean Jakoncic of NSLS beamline X6A are thanked. We also thank Dr. Martin Schiller at University of Connecticut Health Center for insight into the structure of SH2 domains.*

## REFERENCES


1. Bradley, W. D., and Koleske, A. J. (2009) Regulation of cell migration and morphogenesis by Abl-family kinases: emerging mechanisms and physiological contexts. *J. Cell Sci.* **122,** 3441–3454
2. Kruh, G. D., Perego, R., Miki, T., and Aaronson, S. A. (1990) The complete coding sequence of Arg defines the Abelson subfamily of cytoplasmic tyrosine kinases. *Proc. Natl. Acad. Sci. U.S.A.* **87,** 5802–5806
3. Peacock, J. G., Couch, B. A., and Koleske, A. J. (2010) The Abl and Arg non-receptor tyrosine kinases regulate different zones of stress fiber, focal adhesion, and contractile network localization in spreading fibroblasts. *Cytoskeleton* **67,** 666–675
4. Moresco, E. M., Donaldson, S., Williamson, A., and Koleske, A. J. (2005) Integrin-mediated dendrite branch maintenance requires Abelson (Abl) family kinases. *J Neurosci* **25,** 6105–6118
5. Mader, C. C., Oser, M., Magalhaes, M. A., Bravo-Cordero, J. J., Condeelis, J., Koleske, A. J., and Gil-Henn, H. (2011) An EGFR-Src-Arg-cortactin pathway mediates functional maturation of invadopodia and breast cancer cell invasion. *Cancer Res.* **71,** 1730–1741
6. Koleske, A. J., Gifford, A. M., Scott, M. L., Nee, M., Bronson, R. T., Miczek, K. A., and Baltimore, D. (1998) Essential roles for the Abl and Arg tyrosine kinases in neurulation. *Neuron* **21,** 1259–1272
7. Müller, R., Slamon, D. J., Tremblay, J. M., Cline, M. J., and Verma, I. M. (1982) Differential expression of cellular oncogenes during pre- and postnatal development of the mouse. *Nature* **299,** 640–644
8. Renshaw, M. W., Capozza, M. A., and Wang, J. Y. (1988) Differential expression of type-specific c-abl mRNAs in mouse tissues and cell lines. *Mol. Cell Biol.* **8,** 4547–4551
9. Perego, R., Ron, D., and Kruh, G. D. (1991) Arg encodes a widely expressed 145 kDa protein-tyrosine kinase. *Oncogene* **6,** 1899–1902
10. Lapetina, S., Mader, C. C., Machida, K., Mayer, B. J., and Koleske, A. J. (2009) Arg interacts with cortactin to promote adhesion-dependent cell edge protrusion. *J. Cell Biol.* **185,** 503–519
11. Boyle, S. N., Michaud, G. A., Schweitzer, B., Predki, P. F., and Koleske, A. J. (2007) A critical role for cortactin phosphorylation by Abl-family kinases in PDGF-induced dorsal-wave formation. *Curr. Biol.* **17,** 445–451
12. Liu, W., MacGrath, S. M., Koleske, A. J., and Boggon, T. J. (2012) Lysozyme contamination facilitates crystallization of a heterotrimeric cortactin-Arg-lysozyme complex. *Acta Crystallogr. Sect. F Struct. Biol. Cryst. Commun.* **68,** 154–158
13. Martin, K. H., Jeffery, E. D., Grigera, P. R., Shabanowitz, J., Hunt, D. F., and Parsons, J. T. (2006) Cortactin phosphorylation sites mapped by mass spectrometry. *J. Cell Sci.* **119,** 2851–2853
14. Huang, C., Liu, J., Haudenschild, C. C., and Zhan, X. (1998) The role of tyrosine phosphorylation of cortactin in the locomotion of endothelial cells. *J. Biol. Chem.* **273,** 25770–25776
15. MacGrath, S. M., and Koleske, A. J. (2012) Cortactin in cell migration and cancer at a glance. *J. Cell Sci.* **125,** 1621–1626
16. Huang, H., Li, L., Wu, C., Schibli, D., Colwill, K., Ma, S., Li, C., Roy, P., Ho, K., Songyang, Z., Pawson, T., Gao, Y., and Li, S. S. (2008) Defining the specificity space of the human SRC homology 2 domain. *Mol. Cell Proteomics* **7,** 768–784
17. Songyang, Z., Shoelson, S. E., Chaudhuri, M., Gish, G., Pawson, T., Haser, W. G., King, F., Roberts, T., Ratnofsky, S., and Lechleider, R. J. (1993) SH2 domains recognize specific phosphopeptide sequences. *Cell* **72,** 767–778
18. Kaneko, T., Huang, H., Zhao, B., Li, L., Liu, H., Voss, C. K., Wu, C., Schiller, M. R., and Li, S. S. (2010) Loops govern SH2 domain specificity by controlling access to binding pockets. *Sci. Signal.* **3,** ra34
19. Liu, B. A., Jablonowski, K., Shah, E. E., Engelmann, B. W., Jones, R. B., and Nash, P. D. (2010) SH2 domains recognize contextual peptide sequence information to determine selectivity. *Mol. Cell Proteomics* **9,** 2391–2404
20. Otwinowski, Z., and Minor, W. (1997) Processing of x-ray diffraction data collected in oscillation mode. *Macromol. Crystallogr. A* **276,** 307–326
21. McCoy, A. J., Grosse-Kunstleve, R. W., Storoni, L. C., and Read, R. J. (2005) Likelihood-enhanced fast translation functions. *Acta Crystallogr. D Biol. Crystallogr.* **61,** 458–464
22. Wojcik, J., Hantschel, O., Grebien, F., Kaupe, I., Bennett, K. L., Barkinge, J., Jones, R. B., Koide, A., Superti-Furga, G., and Koide, S. (2010) A potent and highly specific FN3 monobody inhibitor of the Abl SH2 domain. *Nat. Struct. Mol. Biol.* **17,** 519–527
23. Perrakis, A., Harkiolaki, M., Wilson, K. S., and Lamzin, V. S. (2001) ARP/wARP and molecular replacement. *Acta Crystallogr. D Biol. Crystallogr.* **57,** 1445–1450
24. Emsley, P., and Cowtan, K. (2004) Coot: model-building tools for molecular graphics. *Acta Crystallogr. D Biol. Crystallogr.* **60,** 2126–2132
25. Murshudov, G. N., Vagin, A. A., and Dodson, E. J. (1997) Refinement of macromolecular structures by the maximum-likelihood method. *Acta Crystallogr. D Biol. Crystallogr.* **53,** 240–255
26. Perrakis, A., Morris, R., and Lamzin, V. S. (1999) Automated protein model building combined with iterative structure refinement. *Nat. Struct. Biol.* **6,** 458–463
27. Laskowski, R. A., MacArthur, M. W., Moss, D. S., Thornton, J. M. (1993) PROCHECK: a program to check the stereochemical quality of protein structures. *J. Appl. Crystallogr.* **26,** 283–291
28. Chen, V. B., Arendall, W. B., 3rd, Headd, J. J., Keedy, D. A., Immormino, R. M., Kapral, G. J., Murray, L. W., Richardson, J. S., and Richardson, D. C.

(2010) MolProbity: all-atom structure validation for macromolecular crystallography. *Acta Crystallogr. D Biol. Crystallogr.* **66,** 12–21
29. Kabsch, W., and Sander, C. (1983) Dictionary of protein secondary structure: pattern recognition of hydrogen-bonded and geometrical features. *Biopolymers* **22,** 2577–2637
30. Miller, A. L., Wang, Y., Mooseker, M. S., and Koleske, A. J. (2004) The Abl-related gene (Arg) requires its F-actin-microtubule cross-linking activity to regulate lamellipodial dynamics during fibroblast adhesion. *J. Cell Biol.* **165,** 407–419
31. Nagar, B., Hantschel, O., Seeliger, M., Davies, J. M., Weis, W. I., Superti-Furga, G., and Kuriyan, J. (2006) Organization of the SH3-SH2 unit in active and inactive forms of the c-Abl tyrosine kinase. *Mol. Cell* **21,** 787–798
32. Nagar, B., Hantschel, O., Young, M. A., Scheffzek, K., Veach, D., Bornmann, W., Clarkson, B., Superti-Furga, G., and Kuriyan, J. (2003) Structural basis for the autoinhibition of c-Abl tyrosine kinase. *Cell* **112,** 859–871
33. Nam, H. J., Haser, W. G., Roberts, T. M., and Frederick, C. A. (1996) Intramolecular interactions of the regulatory domains of the Bcr-Abl kinase reveal a novel control mechanism. *Structure* **4,** 1105–1114
34. Overduin, M., Rios, C. B., Mayer, B. J., Baltimore, D., and Cowburn, D. (1992) Three-dimensional solution structure of the Src homology 2 domain of c-abl. *Cell* **70,** 697–704
35. Eck, M. J., Shoelson, S. E., and Harrison, S. C. (1993) Recognition of a high-affinity phosphotyrosyl peptide by the Src homology-2 domain of p56lck. *Nature* **362,** 87–91
36. Metzler, W. J., Leiting, B., Pryor, K., Mueller, L., and Farmer, B. T., 2nd. (1996) The three-dimensional solution structure of the SH2 domain from p55blk kinase. *Biochemistry* **35,** 6201–6211
37. Schindler, T., Sicheri, F., Pico, A., Gazit, A., Levitzki, A., and Kuriyan, J. (1999) Crystal structure of Hck in complex with a Src family-selective tyrosine kinase inhibitor. *Mol. Cell* **3,** 639–648
38. Arold, S. T., Ulmer, T. S., Mulhern, T. D., Werner, J. M., Ladbury, J. E., Campbell, I. D., and Noble, M. E. (2001) The role of the Src homology 3-Src homology 2 interface in the regulation of Src kinases. *J. Biol. Chem.* **276,** 17199–17205
39. Gilmer, T., Rodriguez, M., Jordan, S., Crosby, R., Alligood, K., Green, M., Kimery, M., Wagner, C., Kinder, D., and Charifson, P. (1994) Peptide inhibitors of Src SH3-SH2-phosphoprotein interactions. *J. Biol. Chem.* **269,** 31711–31719
40. Tong, L., Warren, T. C., King, J., Betageri, R., Rose, J., and Jakes, S. (1996) Crystal structures of the human p56lck SH2 domain in complex with two short phosphotyrosyl peptides at 1.0 Å and 1.8 Å resolution. *J. Mol. Biol.* **256,** 601–610
41. Miller, M. M., Lapetina, S., MacGrath, S. M., Sfakianos, M. K., Pollard, T. D., and Koleske, A. J. (2010) Regulation of actin polymerization and adhesion-dependent cell edge protrusion by the Abl-related gene (Arg) tyrosine kinase and N-WASp. *Biochemistry* **49,** 2227–2234
42. Oser, M., Mader, C. C., Gil-Henn, H., Magalhaes, M., Bravo-Cordero, J. J., Koleske, A. J., and Condeelis, J. (2010) Specific tyrosine phosphorylation sites on cortactin regulate Nck1-dependent actin polymerization in invadopodia. *J. Cell Sci.* **123,** 3662–3673
43. Butler, B., Kastendieck, D. H., and Cooper, J. A. (2008) Differently phosphorylated forms of the cortactin homolog HS1 mediate distinct functions in natural killer cells. *Nat. Immunol.* **9,** 887–897
44. Wang, Y., Miller, A. L., Mooseker, M. S., and Koleske, A. J. (2001) The Abl-related gene (Arg) nonreceptor tyrosine kinase uses two F-actin-binding domains to bundle F-actin. *Proc. Natl. Acad. Sci. U.S.A.* **98,** 14865–14870
45. Mayer, B. J., and Baltimore, D. (1994) Mutagenic analysis of the roles of SH2 and SH3 domains in regulation of the Abl tyrosine kinase. *Mol. Cell Biol.* **14,** 2883–2894
46. Mayer, B. J., Hirai, H., and Sakai, R. (1995) Evidence that SH2 domains promote processive phosphorylation by protein-tyrosine kinases. *Curr. Biol.* **5,** 296–305
47. Pellicena, P., Stowell, K. R., and Miller, W. T. (1998) Enhanced phosphorylation of Src family kinase substrates containing SH2 domain binding sites. *J. Biol. Chem.* **273,** 15325–15328
48. Potterton, L., McNicholas, S., Krissinel, E., Gruber, J., Cowtan, K., Emsley, P., Murshudov, G. N., Cohen, S., Perrakis, A., and Noble, M. (2004) Developments in the CCP4 molecular-graphics project. *Acta Crystallogr. D Biol. Crystallogr.* **60,** 2288–2294